Fine-Tuning the optoelectronic and redox properties of an electropolymerized thiophene derivative for highly selective OECT-based zinc detection

Tommaso Nicolini, Shekhar Shinde, Reem El-Attar, Gerardo Salinas, Damien Thuau, Mamatimin Abbas, Matthieu Raoux, Jochen Lang, Eric Cloutet, Alexander Kuhn

Fine-Tuning the optoelectronic and redox properties of an electropolymerized thiophene derivative for highly selective OECT-based zinc detection

*Tommaso Nicolini, Shekhar Shinde, Reem El-Attar, Gerardo Salinas, Damien Thuau, Mamatimin Abbas, Matthieu Raoux, Jochen Lang, Eric Cloutet, Alexander Kuhn**

Dr. T. Nicolini, Dr. G. Salinas, Prof. A. Kuhn
Univ. Bordeaux, CNRS, Bordeaux INP, ISM, UMR 5255, 33607 Pessac, France
E-mail: kuhn@enscbp.fr

Dr. S. Shinde, Dr. E. Cloutet
Uni. Bordeaux, CNRS, Bordeaux INP, LCPO, UMR 5629, 33615 Pessac, France

R. El-Attar, Dr. D. Thuau, Dr. M. Abbas
Univ. Bordeaux, CNRS, Bordeaux INP, IMS, UMR 5218, 33607 Pessac, France

Prof. M. Raoux, Prof. J. Lang,
Univ. Bordeaux, CNRS, Bordeaux INP, CBMN, UMR 5248, 33600 Pessac, France

Keywords: conducting polymers, cation detection, sensitivity, selectivity, electrochemical conductance, OECT

Abstract

Organic mixed ionic-electronic conductors (OMIEC) have emerged as pivotal materials in organic bioelectronics, particularly when integrated into organic electrochemical transistors (OECTs). Conducting polymer-based devices have indeed demonstrated their capability to transduce biological signals into amplified output signals, harnessing the high transconductance of OECTs. The OECT operating principle and sensing capability strongly depends on ion-conjugated backbone coupling: the dual nature of OMIECs, i.e. ion-conductor and electron/hole-conductor, presents an intrinsic interface in the bulk of the thin film across which transduction of ionic signals into electronic signals and *vice versa* occurs. Recent works have shown how selective sodium and potassium detection can be achieved by direct chemical modification of the polymer. Such modifications introduce ligands with affinity for the cations of interest as substituents on the

polymer chain. The present work explores the integration of specifically modified conducting polymers into OECT channels, offering selectivity for zinc cations. Zinc fluxes are crucial in various biological processes, and their reliable detection, especially at low concentrations, is an important challenge. By electropolymerizing a thiophene-based trimer, modified with a dipicolylamine (DPA) substituent, we obtain a conducting polymer-based OECT that can selectively detect Zn^{2+} in the 10^{-6} to 10^{-3} mol L^{-1} concentration range in physiological buffers.

1. Introduction

Bioelectronics[1] holds great promise for developing a new generation of medical devices that will allow advances in diagnostics, monitoring and treatment of diseases and conditions. Due to their ionic and electronic conductivity, as well as their mechanical properties, conducting polymers have been at the forefront of organic bioelectronics[2], especially when integrated as active materials in organic electrochemical transistors[3] (OECTs). The necessary requirements for a conducting polymer to be used in OECTs is that it should behave as an organic mixed ion/electron conductor (OMIEC).[4]

During OECT operation, the OMIEC has to be able to undergo reversible electrochemical doping/dedoping in a given electrolyte, e.g. aqueous electrolyte for bioelectronics applications[5]. OMIEC-based devices have already shown the ability to transduce biological signals, related e.g. to ion fluxes occurring among cells, into an amplified output signal[6]. Their amplification power, stemming from the high transconductance[7] of OECTs, has also been exploited to develop analytical methods[8] with sensitivities that rival most advanced electrochemical methods, even without the need of a Faraday cage[9].

OECT sensing capabilities[8] are based on the interaction of an analyte with either the channel or the gate electrode and the resulting modulation of the transistor readout, i.e. the drain current, I_d. The working principle of these devices for detecting a specific target analyte is mainly based on either amperometric or potentiometric sensing[10] to quantify selectively redox active biological molecules or ionic species in solution, respectively, coupled to the intrinsic amplification power of OECTs. These endeavors have been generally achieved by functionalization of the gate electrode or channel materials with antibodies[11,12,13,14] or enzymes[15,16,17,18] having specific interactions or catalytic activity towards a target molecule of biological interest. Customized materials, which show preferential catalytic redox activity for specific biological molecules[19], or which can be used as ion-selective membranes, have been employed in this context for specific cation sensing.[20,21,22]

Since the electrochemical doping/dedoping process is intimately governed by ion-aromatic backbone coupling[23], an alternative route to achieve selectivity towards cations of biological interest involves adding this functionality to the conducting polymer through direct chemical modification. A few examples of exploring this strategy have revealed that the electrochemical doping/dedoping of OMIECs can be influenced, allowing discrimination between sodium and potassium in the electrolyte, based on the introduction of crown ether substituents on the OMIEC backbone.[24,25,26]

For example, OECT-based membrane-free specific cation sensing has been achieved by implementing poly(3,4-alkoxy thiophene) (PEDOT) derivatives with added functionality at the gate electrode of an OECT through electropolymerization. In this work[24], Wustoni *et al.* obtained devices that could monitor potassium and sodium concentration changes in human serum thanks to the specific interaction between the target cation and the modified gate surface. More specifically, a pseudo-Nernstian relationship between the concentration of the target cation and the

output current of the OECTs could be determined, showing detection limits of 10^{-4} mol L^{-1} for potassium and 10^{-5} mol L^{-1} for sodium, as well as linear regimes between 10^{-4} and 10^{-1} mol L^{-1}, comparable to state-of-the-art OECT devices employing ion-selective membranes.

Through a similar chemical modification, Salinas *et al.* showed that the interaction between sodium and a crown ether substituent has a specific effect on the evolution of the electrical conductivity[26] of the modified OMIEC and could therefore be exploited to determine if sodium is present in the electrolyte. These results suggest the possibility of integrating a modified conducting polymer with selectivity towards a specific target cation in the channel of an OECT.

In its cationic form, zinc plays key-roles in numerous biological processes[27,28] relevant to the immune, nervous and endocrine systems, as well as in the metabolism of RNA and DNA. Therefore, the development of methods for detecting and monitoring its dynamic concentrations is currently investigated intensively to provide tools for biological and medical *in vivo* or *in vitro* studies. Dipicolylamine (DPA) is a well-known complexing agent of transition metals[29,30,31] in general and has been successfully used to detect zinc mainly by fluorescence techniques[32], also in cell cultures[33].

In this work, we present the design of a novel OMIEC that is able to detect zinc ions in aqueous solutions when implemented as a channel material of an OECT (see **Figure 1**). The OMIEC is obtained by electropolymerization of an aromatic precursor based on a thiophene trimer, more specifically 2,5-bis(3,4-ethylenedioxy thiophene)thiophene, already used as a platform for other OECTs[34] and bioelectronics[35,36] applications. The interaction that allows a specific response towards zinc is achieved by the chemical modification of the thiophene-based trimer with a DPA substituent. The resulting molecule is 2-(bis(pyridin-2-ylmethyl)amino)ethyl 2-(2,5-bis(3,4-ethylenedioxy thiophene)thiophen-3-yl)acetate and from here on will be referred to as Tri-DPA.

Through electropolymerization of Tri-DPA in the presence of zinc cations, we obtained a conducting polymer that we label Zn-templated pTri-DPA. This polymer can reversibly switch between its conducting and insulating state in aqueous solutions, and also in biological buffers typically used in cell cultures. Most importantly, we integrate this conducting polymer in OECT devices and demonstrate its selectivity towards zinc with respect to other cations usually present in biological media. To the best of our knowledge, this is the first example of an OECT showing specific detection of this biologically relevant cation. Moreover, we show how changes in zinc concentration as low as 1.5 µM can be detected, i.e. one order of magnitude lower than what has been achieved for potassium and sodium with other membrane-free OECT-based sensing techniques[24].

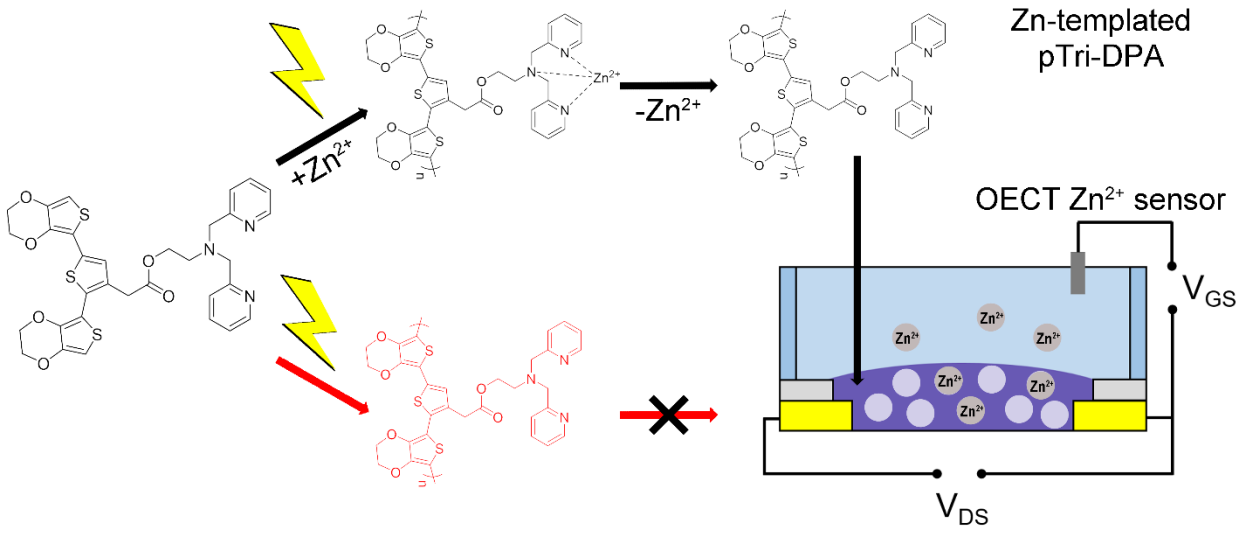

Figure 1. Scheme representing the process to obtain Zn-templated pTri-DPA and the sensing principle allowing its use as active material in OECT-based Zn^{2+} sensors in aqueous solutions.

2. Results and discussion

2.1 Electropolymerization of the Tri-DPA:Zn^{2+} complex

First, we synthesized and characterized Tri-DPA and analogs (synthesis and chemical characterization details are reported in SI – see Figures S1-10). In order to ensure that the interaction between zinc and DPA is retained by our precursor, we performed NMR titrations by adding the target cation to a solution of Tri-DPA. As zinc equivalents are increased from 0 to 1, most ^{1}H peaks present changes in chemical shift and intensity (see Figure S11), confirming the formation of a complex. Since DPA and zinc can form both 1:1 and a 2:1 host-guest complexes[37], we could not determine a reliable value for the binding constant. However, the observed changes of the NMR spectrum of Tri-DPA when zinc equivalents are added to the solution suggest that the interactions between the cation and DPA is retained by the precursor.

The subsequent step to obtain the conducting polymer consisted in the electropolymerization of Tri-DPA by oxidation of the thiophene-based trimer. However, the DPA moiety is itself redox active and the products of secondary and tertiary amine oxidation can undergo further irreversible reactions, leading to bond cleavage[38]. This would result in the degradation of the DPA moiety and the loss of the zinc binding functionality. Interestingly, we noticed that the redox transformation of DPA can be prevented when this molecule is complexed by Zn^{2+} (see Figure S12).

Therefore, we investigated the effect of adding increasing Zn equivalents during electropolymerization in an acetonitrile (ACN) solution of 5 mmol L^{-1} Tri-DPA and 100 mmol L^{-1} of tetrabutyl ammonium perchlorate (TBAP) as supporting electrolyte on the final electrochemical and optical properties of pTri-DPA films. Cyclic voltammetry (CV) experiments of such solutions containing 1.25, 2.5 and 5 mmol L^{-1} of $Zn(ClO_4)_2$ showed partial or complete suppression of the anodic processes related to DPA oxidation (see Figure S13A). As perchlorate is the counter-anion of the supporting electrolyte, $Zn(ClO_4)_2$ has been chosen as the Zn^{2+} source to

avoid mixed anion effects. The prevention of this competing oxidation should beneficially affect the electropolymerization process and the final properties of the conducting polymer layer.

Preliminary inspection of pTri-DPA films obtained by potentiostatic deposition (see details for chronoamperometric recordings of the electropolymerization experiments in SI and Figure S13B) in the presence of 0, 0.25, 0.5 and 1 Zn equivalents showed a color gradient for such films (see Figure S14A). This evidence suggests a correlation between the polymer's optoelectronic properties and Zn content of the electropolymerization solution, quantified in terms of a bathochromic absorption maxima, $\lambda_{abs\ max}$ shift measured by UV/vis spectroscopy (see Figure S14B). Such a red shift can be ascribed to a longer effective conjugation length, usually associated with a minimization of torsional defects of conducting polymer backbone in the solid thin-film structure[39].

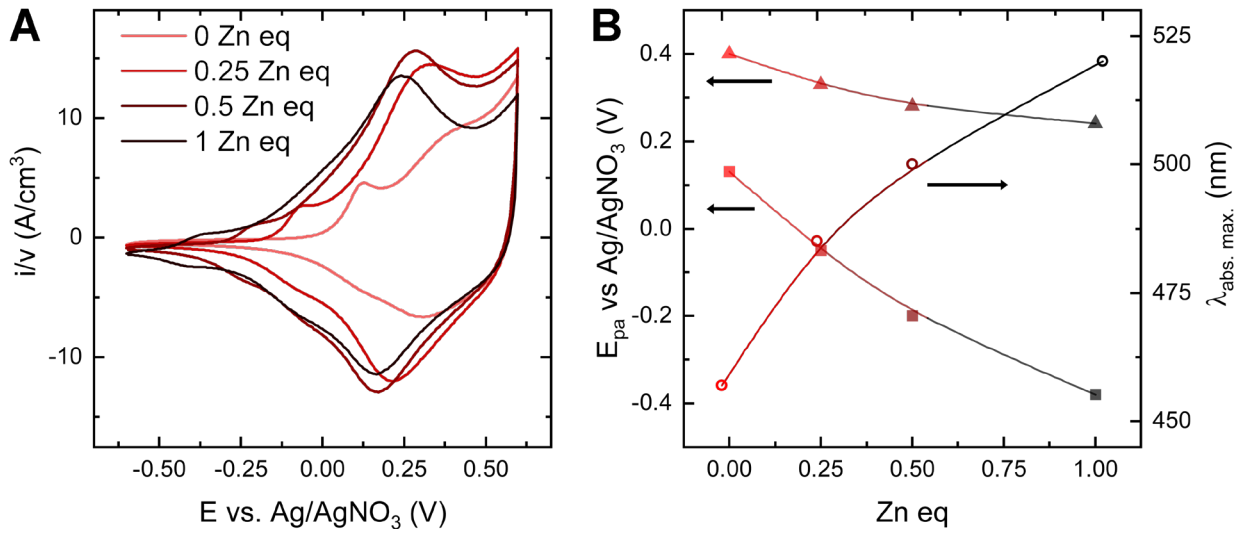

Figure 2. A) CVs measured in an ACN solution of 100 mmol L^{-1} TBAP of pTri-DPA films obtained by electropolymerization in the presence of increasing Zn equivalents, (gradient from red to black for electropolymerization solutions containing 0, 0.25, 0.5, and 1 Zn equivalents); B) anodic peak potentials related to the

doping process of pTri-DPA extracted from the CV curves in A (squares and triangles – left axis) and absorption maxima wavelengths (circles – right axis) from Figure S14B plotted against Zn equivalents present during electropolymerization. Lines are guides to the eye to show the decrease in the required potential to oxidize pTri-DPA and the increase in absorption wavelength. Currents are normalized by volume, v, calculated from the electrode area in cm^2 and the thickness of the polymer films in cm (ranging from 70 nm to 90 nm) as determined by profilometry.

The spectroscopic evidence above suggests that adding Zn ions to the electropolymerization solution results in a beneficial effect in terms of a better planarity of the polymer chains, which should facilitate the oxidation of the conducting polymer in the solid state[40]. Indeed, the electrochemical characterization of these films by means of CV in a 100 mmol L^{-1} TBAP/ACN solution supports our hypothesis: as Zn equivalents increase, the anodic peak potential, E_{pa}, related to the doping of pTri-DPA shifts towards more negative potentials (see **Figure 2A**).

The effects of adding Zn equivalents on both, the final optoelectronic and redox properties of pTri-DPA are summarized in **Figure 2B,** indicating the decrease in the potential required to oxidize the polymer and the concurrent increase of the UV/vis absorption maxima. In order to ensure that these effects are indeed due to the formation of the Tri-DPA:Zn^{2+} complex prior to electropolymerization, we performed a control experiment with a trimer molecule that bears a substituent (i.e. methyl ester group) that should not show any interaction with zinc. More specifically, Tri-COOMe (see synthesis details in SI, Figures S9-10) was electropolymerized in the presence of increasing Zn equivalents to yield pTri-COOMe films, that were then characterized electrochemically (see Figure S15). No effect on the redox properties is observed, ensuring that the previous behavior is specific to Tri-DPA and not due to a generic effect of Zn^{2+} on the electropolymerization of the trimer.

Prior to characterizing and comparing further the two polymers obtained in the absence and in the presence of Zn^{2+}, named from this point forward pTri-DPA and Zn-templated pTri-DPA,

respectively, we electrochemically extracted Zn^{2+} from the latter to clear the DPA sites, which will be needed later for detecting zinc cations. It is well known[41] that organic mixed conductors undergo swelling and shrinking during electrochemical doping/dedoping since the charging/discharging process of the conjugated backbone is accompanied by injection and expulsion of electrolyte ions and solvent molecules.[42,43,44,45] We expect that the swollen state will provide pathways for zinc ions to leave the polymer. We therefore cycled the polymer 20 times in a Zn-free TBAP/ACN solution under vigorous stirring between +0.4 and -0.6 V, stopping the CV experiment at the positive potential to ensure an additional electrostatic repulsion of the zinc ions. A slow scan rate (≈ 0.01 V s^{-1}) was used in order to give time to the polymer layer to swell and shrink in a controlled fashion, allowing zinc to diffuse out of the organic semiconductor film, while avoiding detrimental effects on its microstructure and electrical properties. In order to confirm the efficient removal of Zn^{2+} from the Zn-templated pTri-DPA, Energy Dispersive X-ray Spectroscopy (EDX) was carried out on three gold wires modified with 1) as-prepared pTri-DPA, 2) as-prepared Zn-templated pTri-DPA, and 3) Zn-templated pTri-DPA cycled in a Zn-free TBAP/ACN solution. EDX data (reported in Figure S16 along with experimental details) reveal that for the latter sample the peak intensity for Zn L-edge is more than halved, suggesting that a large fraction of Zn^{2+} cations has been removed.

2.2 *In-situ* electrochemical conductance of pTri-DPA and Zn-templated pTri-DPA in organic and aqueous electrolytes.

We further investigated the differences between the pTri-DPA and Zn-templated pTri-DPA-based polymers by using the *in-situ* electrochemical conductance technique[46],[47]. This technique allows monitoring the evolution of conductance measured across interdigitated microelectrode arrays

(IDMEAs) by applying a small potential difference (V_d between 10 and 50 mV) with a potentiostat, while a second potentiostat performs the electrochemistry measurement. It can therefore be used to extract information about the electrical properties of the polymer layer during its formation or simply the charging/discharging of the electroactive material. Importantly, it allows to evaluate the onset potential of the insulating/conducting transition and simultaneously address polymer stability with respect to electrochemical cycling, both relevant material characteristics for applications of electroactive materials as biosensors.

First, we performed electropolymerization of Tri-DPA in the absence and in the presence of Zn^{2+} (2 Zn equivalents) on gold IDMEA by potentiostatic deposition with an electrochemical conductance setup, consisting of two potentiostats (see details in SI). A rather high concentration of Zn^{2+} with respect to Tri-DPA was used in order to ensure that 1) all DPA sites are protected by the target cation, and 2) the most prevalent complex species would be the 1:1 host:guest thanks to the excess of Zn^{2+} in solution. The evolution of the charge related to the oxidation of Tri-DPA and Tri-DPA:Zn^{2+}, prompted by applying 0.4 V vs. $Ag/AgNO_3$ with the first potentiostat, is shown in Figure 3A (see red and black dashed lines representing the charge for Tri-DPA and Tri-DPA:Zn^{2+}, respectively) and can be considered proportional to the amount of deposited polymer. Under these conditions, electrodeposition will initially occur on the surface of the microelectrodes. Therefore, monitoring the current flowing between the two terminals of the IDMEA with the second potentiostat will yield low conductance. As the amount of deposited polymer increases, connections will start to form across the gap between microelectrodes, causing a steep increase in conductance[46,48]. Finally, a saturation region is reached where conductance increases slowly as the thin polymer layer across the gap grows vertically. The conductance evolution shown in Figure 3A allows two observations: 1) a smaller amount of deposited charge is required to get to the saturation

region for Tri-DPA:Zn^{2+} than for Tri-DPA, and 2) the maximum conductance value reached is roughly twice in the case of polymerization of the Zn complex. The first effect can be explained by considering that the deposited charge measured during the electropolymerization process is related to all anodic processes occurring at the IDMEA surface. When free Tri-DPA is present in solution, both the conjugated trimer and the DPA moiety are oxidized. However, the latter oxidation process is prevented when Zn protects the DPA moiety. This allows avoiding deposition of a polymer with a degraded molecular recognition unit. The second observation concerning the maximum conductance value reached could be rationalized in terms of an overall better conductivity of the final polymer, which depends on the amount of charge carriers that can be stored on the conjugated backbone and their mobility, for the same amount of deposited polymer. These properties of conducting polymers are generally enhanced when the effective conjugation length of their π-system is increased.

Rationalization of the observed behavior implies that for the same deposited charge, the amount of deposited polymer should be higher for electropolymerization conducted in the presence of Zn^{2+}, i.e. when oxidation of DPA is prevented and the measured charge relates mostly to the oxidation of the trimer moiety. This is confirmed by measuring the thickness of polymer layers obtained for different deposition charge values while varying the Zn^{2+} equivalents. The polymer films electrodeposited in the absence of Zn^{2+} are systematically half as thick as those obtained when this cation is present in solution (see Figure S17 and details in SI). Therefore, we can consider both observations consistent with our hypothesis, previously deduced from the electrochemical and spectroscopic characterization of the films, that the electropolymerization of Tri-DPA:Zn^{2+} leads to a more planar and defect-free conjugated backbone structure.

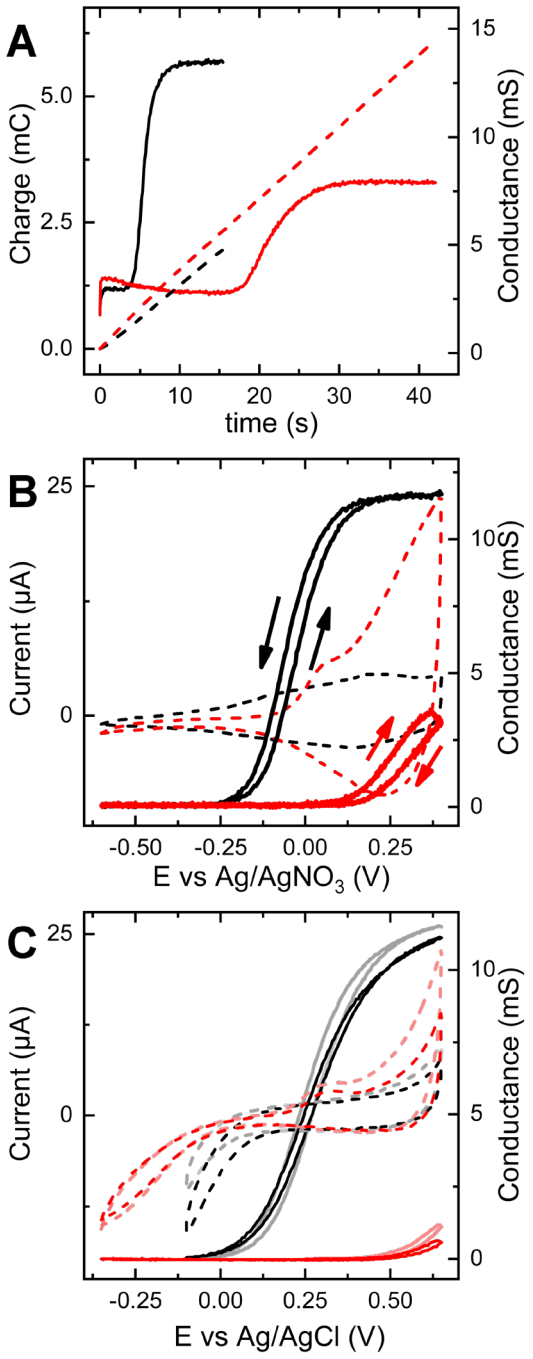

Figure 3. A) Deposited charge recorded during electropolymerization of Tri-DPA and Tri-DPA:Zn^{2+} (red and black dashed lines, respectively) on Pt IDMEAs and the simultaneously recorded conductance (red and black solid lines, respectively); B,C) Evolution of the conductance during electrochemical cycling of pTri-DPA and Zn-templated pTri-DPA, shown in red and black, respectively (solid lines represent conductance and dashed lines represent CV traces) in B) a 100 mmol L^{-1} TBAP/ACN solution (E_{min} = -0.6 V; E_{max} = 0.4 V vs. $Ag/AgNO_3$ ν = 0.01 V s^{-1}, ΔV = 10 mV); and

in C) an aqueous buffer solution used in typical cell cultures (E_{min} = -0.35 V; E_{max} = 0.65 V vs. Ag/AgCl in sat KCl ν = 0.01 V s^{-1}, ΔV = 10 mV). Data obtained in aqueous buffer solution show the 1st and 10th cycles in light and dark coloring, respectively).

We then went on to compare the electrochemical conductance of a pTri-DPA film with a Zn-templated pTri-DPA film after the electrochemical removal of Zn^{2+}. The CVs of **Figure 3B** show that the onset potential, E_{onset}, required for the transition from the insulating to the conducting state, shifts to much lower values for the Zn-templated polymer as opposed to pTri-DPA. The large negative shift of the low potential anodic peak of pTri-DPA ($\Delta E_{pa} \approx$ -0.35 V) is quite promising to assure that the transition of the polymer from its insulating to its conducting state, which is driven electrochemically in an OECT, falls within the electrochemical stability window of an aqueous electrolyte. Due to this shift, it is not possible to precisely determine the saturation conductance for non-templated pTri-DPA because a degradation process occurs that causes a 25% decrease in maximum conductance when its conductivity is probed beyond 0.35 V vs. $Ag/AgNO_3$. This is not the case for Zn-templated pTri-DPA, which shows no significant conductance loss when cycled to its highly conductive state (see comparison of normalized conductance evolution in Figure S18 for pTri-DPA and Zn-templated pTri-DPA over 10 cycles).

Next, we performed *in-situ* electrochemical conductance for both polymers using a complex buffer typically used in cell cultures (see buffer composition details in SI) as an electrolyte. **Figure 3C** clearly demonstrates the importance of the Zn-templating effect. While Zn-templated pTri-DPA can be effectively cycled to its conducting state, non-templated pTri-DPA barely switches on, even at a relatively high voltage (E_{max} = 0.65 V vs. Ag/AgCl).

2.3 Electrochemistry of Zn detection with Zn-templated pTri-DPA in a complex physiological buffer.

The encouraging results of the *in-situ* electrochemical conductance measurements allowed moving on to the proof-of-concept experiments with respect to the detection of Zn^{2+} when these polymers are present in the IDMEA channels. While keeping the polymer in its conductive state by applying a relatively low positive voltage (≈ + 0.3 V vs. Ag/AgCl), we expect the measured conductance to drop as we add increasing amounts of Zn^{2+} to the electrolyte buffer solution (see **Figure 4A** and **B**). This drop in conductance should be prompted by the chemical adsorption of the cation due to the interaction with the DPA ligands and the resulting partial reduction of the conjugated backbone, according to the following reaction:

$$pTriDPA^{n+} + xZn^{2+} + 2xe^{-} \rightarrow pTriDPA^{(n-2x)+}{:}xZn^{2+} \qquad \text{(eq. 1)}$$

In **Figure 4C**, we show the current flowing across the IDMEA through the Zn-templated pTri-DPA, measured in three experiments using the biological buffer at pH 7.4 as electrolyte and applying a constant doping potential: 1) blank experiment; 2) adding increasing Zn^{2+} amounts; and 3) removing the chemically adsorbed Zn. In the first experiment, one can observe that potentiostatic electrochemical doping leads to a fast increase in current (dotted light gray line), followed by a slow drift that leads to a marginal increase of the maximum current over 20 minutes. Next, we repeated the same experiment when spiking with Zn^{2+} concentrations from 0 to 20 μM, 200 μM, and 2 mM, under constant stirring. A clear drop is observable at each injection of buffer solution spiked with Zn^{2+} (black solid line). Finally, by doping again in a Zn-free buffer solution, we record the full recovery of the initial current (dark gray solid line).

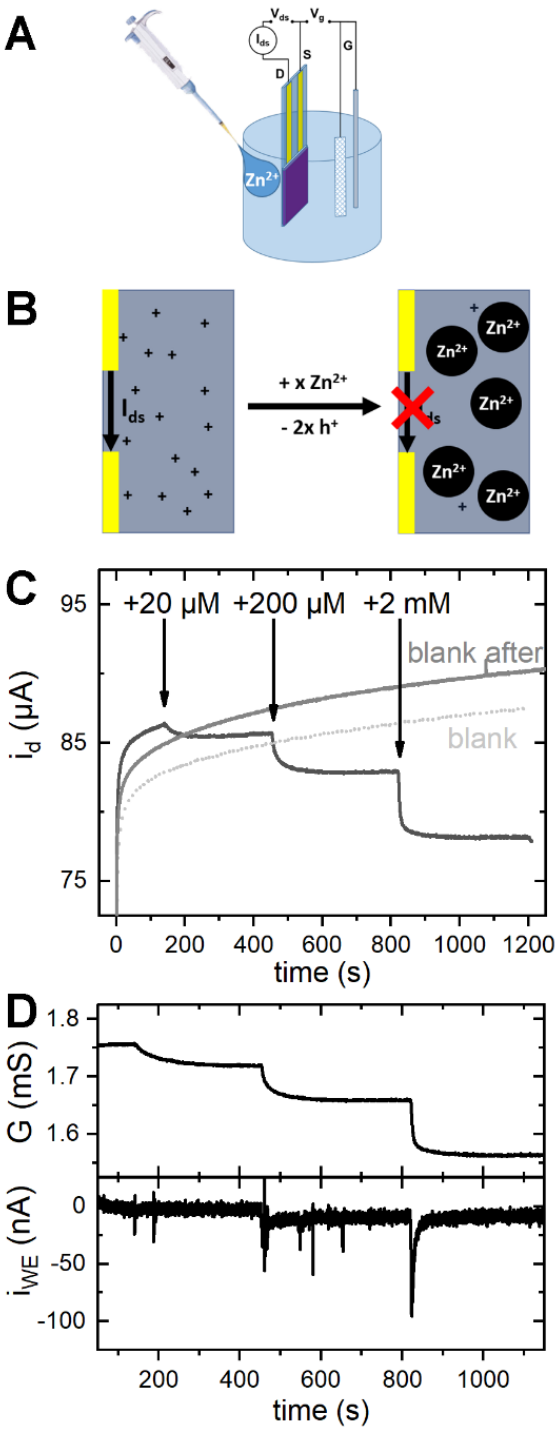

Figure 4. A) Schematics of the *in-situ* electrochemical conductance measurements during Zn additions (working electrode: Pt-IDMEA on which Zn-templated pTri-DPA was electrodeposited, counter electrode: Pt mesh, and reference electrode: Ag/AgCl in saturated KCl); B) Physico-chemical principle of Zn detection with pTri-DPA in its doped state; C) Measurements of the current, i_d, flowing through the Zn-templated pTri-DPA with V_d = 50 mV bias

applied across the IDMEA terminals during application of a doping pulse of + 0.3 V vs Ag/AgCl and sequential addition of Zn^{2+} (at each step the final concentration was 20 µM, 200 µM and 2 mM); D) Conductance evolution, $G = i_d / V_d$, (top panel) and simultaneously recorded current, i_{WE}, (bottom panel) measured by the potentiostat driving the electrochemical doping of the semiconducting polymer.

In **Figure 4D**, we compare the conductance evolution (top panel) during the Zn^{2+} additions corrected for the slow drift and the simultaneously recorded current by the potentiostat applying the constant doping pulse (bottom panel). Overall, an average normalized response of 0.07 dec^{-1} is observed, while the Faradaic current of the IDMEA, serving as a working electrode, shows corresponding cathodic peaks that can be attributed to the reduction of Zn-templated pTri-DPA. Since we are applying a constant doping potential (+0.3 V vs Ag/AgCl), we explain this by the decrease in the doping level of the polymer, prompted by an increase of the effective oxidation voltage required by the polymer once it has absorbed Zn^{2+} cations.

2.4 Miniaturized Zn-templated pTri-DPA OECTs.

After these promising results, we integrated Zn-templated pTri-DPA as channel material into miniaturized OECTs to test their selectivity and determine their sensitivity and detection limit. We electropolymerized the Tri-DPA:Zn^{2+} complex on an OECT substrate with typical channel dimensions of 100 µm in width and 10 µm in length (see fabrication details in SI) and subsequently removed Zn by electrochemical cycling. These steps were performed using the two-potentiostat system of the *in-situ* electrochemical conductance setup as it allows monitoring the formation of the channel and the effect of Zn removal on the conductivity evolution during electrochemical doping/dedoping.

First, we determined electrodeposition conditions by performing a CV and normalizing the current by the surface of the bare source and drain electrodes, which served as the working electrode in a

three-electrode setup with a Pt mesh and a silver wire acting as counter and pseudo-reference electrodes, respectively (see **Figure 5A**). The CV curve shown in **Figure 5B** presents the typical cross-line shape observed for the electropolymerization of thiophene-based conducting polymers[49]. At 0.58 V vs. Ag^+/Ag, we observe a current density *j* of 0.5 mA/cm², which allows for a controlled deposition process. In **Figure 5C**, we show the results of a potentiostatic deposition where the current density starts around the expected value (0.5 mA/cm²) and then steadily increases to tens of mA/cm². This behavior differs greatly from what we observed on large area electrodes or IDMEAs and can be attributed to an edge effect due to the interplay between the diffusion of the redox active species to the source and drain electrode surface and the polymerization reactions occurring with non-oxidized trimers. During the electrodeposition, a small potential difference of 10 mV was applied across the source and drain terminals, to monitor the formation of the channel material with the *in-situ* electrochemical conductance setup. The electropolymerization reaction was stopped when the measured conductance showed values of about 5 mS (see **Figure 5C** – bottom panel) which should yield OECTs with on-currents, i_{ON}, of the order of 0.1 to 1 mA. By integrating the electrodeposition current, we can obtain the deposited charge, which allows estimating the amount of deposited polymer (see **Figure 5C** – top panel).

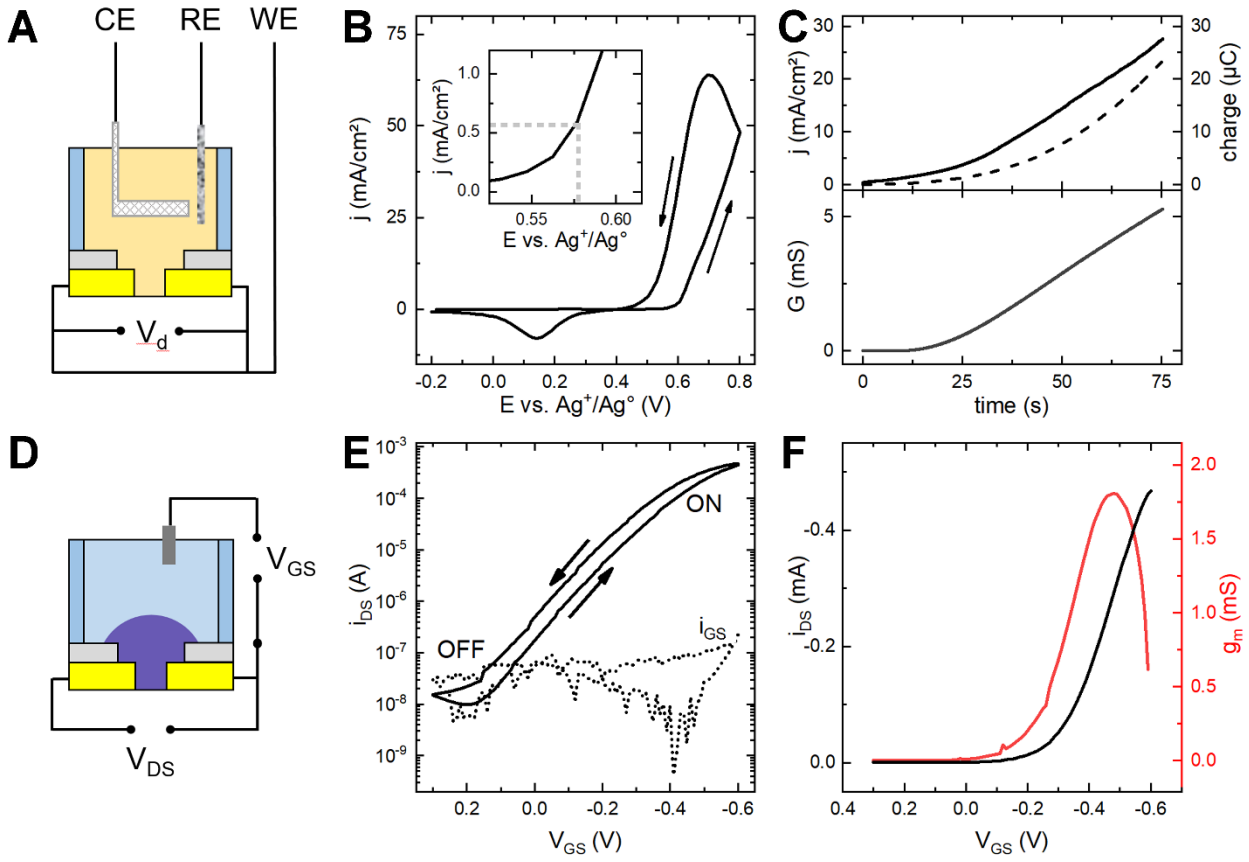

Figure 5. A) Schematics of the *in-situ* electrochemical conductance measurements during electropolymerization conducted in a three-electrode electrochemical cell where source and drain act as the working electrode while a Pt mesh and an Ag wire are used as counter electrode and reference electrode, respectively. The solution used is 10 mmol L^{-1} Tri-DPA:Zn^{2+} in 0.1 mol L^{-1} TBAP/ACN). B) CV curve recorded with a bare OECT substrate (total area of source and drain equals 3000 µm²) to determine deposition conditions (indicated with dashed gray lines) for potentiostatic electropolymerization. The inset shows Tri-DPA oxidation onset; C) Current density *j* recorded during potentiostatic deposition at 0.58 V vs. Ag^+/Ag and the corresponding integrated charge of 24 µC are shown in the top panel while the simultaneously recorded conductance is reported in the bottom panel (V_d = 10 mV); D) Schematics of the OECT characterization setup using an Ag/AgCl pellet as gate electrode (device dimensions: length = 10 µm and width = 100 µm); E) Transfer characteristics on a logarithmic scale obtained at V_{DS} = -0.1 V with i_{ON}/i_{OFF} ratio > 10^4 and negligible gate current, i_{GS}; F) Transfer characteristics showing a transconductance peak of 1.7 mS at V_{GS} = -0.5 V, typical of OECT behavior.

After thoroughly rinsing the devices with ACN and Zn removal by electrochemical cycling in a Zn-free TBAP/ACN solution (see morphological characterization by optical and electron micrographs in Figure S19), we obtained the OECT transfer characteristics using the same aqueous buffer as for the previous *in-situ* conductance measurements in a typical OECT setup, *i.e.* using an Ag/AgCl pellet as gate electrode (see **Figure 5D**). With a high ON/OFF ratio and transconductance of nearly 2 mS at about -0.5 V vs Ag/AgCl (see **Figure 5E** and **F**, respectively), these devices showed promise to detect Zn^{2+} in a complex biological buffer. The values obtained are on par with average OMIEC-based OECTs, which show output currents ranging between 0.1 mA and 10 mA and transconductances between 1 and 10 mS[50].

2.5 Zn Selectivity and sensitivity of pTri-DPA OECTs.

To test the selectivity of Zn-templated pTri-DPA devices, we added Zn^{2+}, Mg^{2+}, Ca^{2+}, and K^{+} to a simple sodium buffer (see composition in SI) at pH = 7.4 while applying a constant doping potential at V_{GS} = -0.35 V. No significant change in the normalized current response, ΔI_{DS}, defined as $(I_{DS}-I_0)/I_0$, is observed for the interfering cations, however Zn^{2+} addition to a final concentration of 550 µmol L^{-1} led to a significant drop in the output current (see **Figure 6A**). We note that the kinetics of the response is relatively slow and we attribute this to the thick nature of the polymer layer constituting the channel. However, a large change occurs in a matter of minutes, i.e. on the same time scale as state-of-the-art devices based on ion exclusion membranes. Additional experiments showed that even by varying concentrations by more than three orders of magnitude, the characteristic response time stays more or less in the same range.

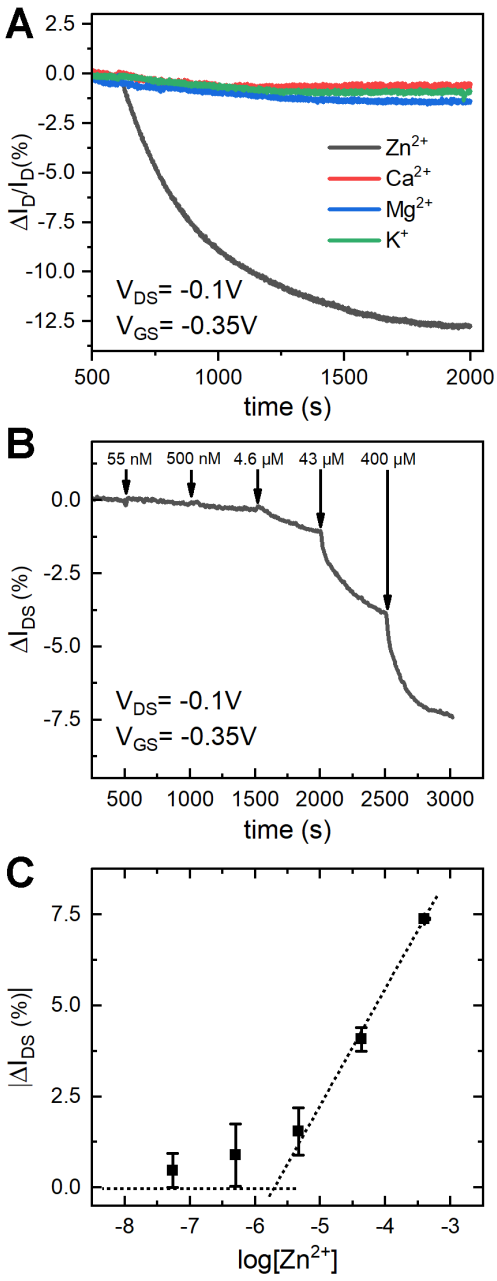

Figure 6. A) Selectivity measurement comparing the normalized current response, ΔI_{DS}, for Zn^{2+}, Mg^{2+}, Ca^{2+}, and K^{+} for 550 µmol L^{-1} (final concentrations) additions. B) Real-time sensitivity measurement for Zn^{2+} concentrations ranging over 5 orders of magnitude. C) Normalized current response, ΔI_{DS}, plotted against the logarithm of the Zn^{2+} concentration. A linear fit (dotted line) to the data points in the 10^{-6} to 10^{-3} concentration range yields a 0.032 dec^{-1} slope and an apparent detection limit of 1.5 µmol L^{-1}, represented by the intersection of dotted lines (see details in SI, Table S1 and S2).

This is nevertheless compatible with real sensing applications as some biological processes, e.g. glucose-stimulated insulin release in pancreatic β-cells involving Zn^{2+} dispersion in extracellular fluids, occur on such time-scales and continue physiologically for 2 to 3 hours. If needed, varying channel dimensions and device geometry[51] is an already proven strategy capable of speeding up the time response of OECTs. Next, we estimated the sensitivity of Zn^{2+} detection by performing consecutive additions in the sodium buffer over a concentration range spanning from 55 nmol L^{-1} to 400 μmol L^{-1}. The evolution of ΔI_{DS} following additions every 500 s is plotted in **Figure 6B**. By measuring the response of three devices, we could determine the relationship between ΔI_{DS} and the logarithm of Zn^{2+} concentration present in the solution in the range between 10^{-6} and 10^{-3} mol L^{-1}. By fitting the data in **Figure 6C**, a slope of 0.032 ± 0.003 dec^{-1} and a lower bound to the limit of detection of 1.5 ± 0.3 μmol L^{-1} is obtained (see data obtained for measurements across three devices and line fitting parameters in Table S1 and Table S2 in SI). This detection limit is comparable with that of fluorescent Zn^{2+}-specific probes used to measure Zn^{2+} release during exocytosis of insulin-containing vesicles from pancreatic β-cells.[52] Our values are on par with what has been achieved for other cations of biological interest, such as sodium and potassium, with membrane-based[20,21,22] or membrane-free[24] OECTs, and this is, to the best of our knowledge, the first demonstration that this type of measurements can be also carried out for Zn^{2+}.

3. Conclusions

OECTs permit to detect even weak biological signals in intact biological systems or micro-organs and open the possibility of detailed analysis of complex biological systems[53,54]. In this work, we present Zn^{2+}-selective OECT sensors based on a novel material consisting of an electropolymerized thiophene derivative trimer, bearing a DPA substituent. The target cation was used in the electropolymerization process to protect the DPA moiety from undesired oxidation, leading to a

highly conductive polymer. The templating effect of Zn^{2+} was beneficial to tune the optoelectronic, electrochemical and electrical properties of pTri-DPA as investigated by spectroscopic, voltametric and *in-situ* electrochemical conductance measurements. Most importantly, the strategy of protecting the complexing group with the target cation itself during the electropolymerization process could open up the possibility of coupling otherwise unexplored redox-active molecules as substituents that might show specific interactions towards analytes of biological interest.

After showing evidence that supports the envisaged physico-chemical principle of Zn^{2+} detection by *in-situ* electrochemical conductance measurements, we proceeded to implement the Zn-templated pTri-DPA in micrometric-sized OECT devices, which showed device characteristics on par with typical OMIEC-based transistor devices operating in aqueous electrolytes. OECT channel formation was monitored during the electropolymerization process in order to deposit the minimal amount of polymer that allowed sufficiently high output currents.

The resulting devices were then successfully employed for the highly selective detection of the target cation in a typical sodium buffer, with no interference from other cations, such as Mg^{2+}, Ca^{2+} and K^{+}, usually present in biological media. This selectivity, coupled with the sensitivity determined for our devices (0.032 dec^{-1} and LoD of 1.5 μmol L^{-1}) makes Zn-templated pTri-DPA a good candidate to develop new OECT platforms for bioelectronics applications. To the best of our knowledge, this is the first time that detection of this target cation has been achieved directly due to the functionality added to the channel material.

Acknowledgements

We acknowledge funding from the ANR project MULTISPOT (ANR-17-CE09-0015 to EC, AK and JL) and the CNRS prematuration project EASYSCREEN (to JL, EC, AK and MA). G.S. is grateful for support via the ERC Advanced grant ELECTRA (No 741251 to AK). The authors also acknowledge the Equipex ELORPrintTec ANR-10-EQPX-28-01 for the microfabrication of the OECTs.

References

[1] P. Chen, X. Sun, H. Peng, *Adv. Funct. Mater.* **2020**, *30*, 2001827.
[2] J. Rivnay, R. M. Owens, G. G. Malliaras, *Chem. Mater.* **2014**, *26*, 679.
[3] J. Rivnay, S. Inal, A. Salleo, R. M. Owens, M. Berggren, G. G. Malliaras, *Nat. Rev. Mater.* **2018**, *3*, 17086.
[4] S. T. M. Tan, A. Gumyusenge, T. J. Quill, G. S. LeCroy, G. E. Bonacchini, I. Denti, A. Salleo, *Adv. Mater.* **2022**, *34*, 2110406.
[5] N. A. Kukhta, A. Marks, C. K. Luscombe, *Chem. Rev.* **2022**, *122*, 4325.
[6] D. T. Simon, E. O. Gabrielsson, K. Tybrandt, M. Berggren, *Chem. Rev.* **2016**, *116*, 13009.
[7] D. Khodagholy, J. Rivnay, M. Sessolo, M. Gurfinkel, P. Leleux, L. H. Jimison, E. Stavrinidou, T. Herve, S. Sanaur, R. M. Owens, G. G. Malliaras, *Nat. Commun.* **2013**, *4*, 2133.
[8] A. Marks, S. Griggs, N. Gasparini, M. Moser, *Adv. Mater. Interfaces* **2022**, *9*, 2102039.
[9] K. Tybrandt, S. B. Kollipara, M. Berggren, *Sensors Actuators B Chem.* **2014**, *195*, 651.
[10] E. Macchia, R. A. Picca, K. Manoli, C. Di Franco, D. Blasi, L. Sarcina, N. Ditaranto, N. Cioffi, R. Österbacka, G. Scamarcio, F. Torricelli, L. Torsi, *Mater. Horizons* **2020**, *7*, 999.
[11] D.-J. Kim, N.-E. Lee, J.-S. Park, I.-J. Park, J.-G. Kim, H. J. Cho, *Biosens. Bioelectron.* **2010**, *25*, 2477.
[12] J. Liu, T. Kong, Y. Xiao, L. Bai, N. Chen, H. Tang, *Biosens. Bioelectron.* **2023**, *230*, 115236.
[13] D. Gentili, P. D'Angelo, F. Militano, R. Mazzei, T. Poerio, M. Brucale, G. Tarabella, S. Bonetti, S. L. Marasso, M. Cocuzza, L. Giorno, S. Iannotta, M. Cavallini, *J. Mater. Chem. B* **2018**, *6*, 5400.
[14] V. Preziosi, M. Barra, V. R. Villella, S. Esposito, P. D'Angelo, S. L. Marasso, M. Cocuzza, A. Cassinese, S. Guido, *Biosensors* **2023**, *13*, 448.
[15] M. E. Welch, T. Doublet, C. Bernard, G. G. Malliaras, C. K. Ober, *J. Polym. Sci. Part A Polym. Chem.* **2015**, *53*, 372.
[16] A. M. Pappa, D. Ohayon, A. Giovannitti, I. P. Maria, A. Savva, I. Uguz, J. Rivnay, I. McCulloch, R. M. Owens, S. Inal, *Sci. Adv.* **2018**, *4*, eaat0911.
[17] C. H. Mak, C. Liao, Y. Fu, M. Zhang, C. Y. Tang, Y. H. Tsang, H. L. W. Chan, F. Yan, *J. Mater. Chem. C* **2015**, *3*, 6532.
[18] O. Parlak, S. T. Keene, A. Marais, V. F. Curto, A. Salleo, *Sci. Adv.* **2018**, *4*, eaar2904.
[19] X. Xi, D. Wu, W. Ji, S. Zhang, W. Tang, Y. Su, X. Guo, R. Liu, *Adv. Funct. Mater.* **2020**, *30*, 1905361.
[20] S. T. Keene, D. Fogarty, R. Cooke, C. D. Casadevall, A. Salleo, O. Parlak, *Adv. Healthc. Mater.* **2019**, *8*, 1901321.
[21] M. Sessolo, J. Rivnay, E. Bandiello, G. G. Malliaras, H. J. Bolink, M. Sessolo, E. Bandiello, H. J. Bolink, J. Rivnay, G. G. Malliaras, *Adv. Mater.* **2014**, *26*, 4803.
[22] Z. Mousavi, A. Ekholm, J. Bobacka, A. Ivaska, *Electroanalysis* **2009**, *21*, 472.
[23] A. Savva, S. Wustoni, S. Inal, *J. Mater. Chem. C* **2018**, *6*, 12023.
[24] S. Wustoni, C. Combe, D. Ohayon, M. Hassan Akhtar, I. McCulloch, S. Inal, S. Wustoni, D. Ohayon, M. H. Akhtar, S. Inal, C. Combe, I. McCulloch, *Adv. Funct. Mater.* **2019**, *29*, 1904403.

[25] A. Villarroel Marquez, G. Salinas, M. Abarkan, M. Idir, C. Brochon, G. Hadziioannou, M. Raoux, A. Kuhn, J. Lang, E. Cloutet, *Macromol. Rapid Commun.* **2020**, *41*, 2000134.
[26] G. Salinas, A. Villarroel Marquez, M. Idir, S. Shinde, B. A. Frontana-Uribe, M. Raoux, J. Lang, E. Cloutet, A. Kuhn, *ChemElectroChem* **2020**, *7*, 2826.
[27] N. Levaot, M. Hershfinkel, *Cell Calcium* **2018**, *75*, 53.
[28] T. Kambe, K. M. Taylor, D. Fu, *J. Biol. Chem.* **2021**, *296*, 100320.
[29] N. Pantalon Juraj, S. Muratović, B. Perić, N. Šijaković Vujičić, R. Vianello, D. Žilić, Z. Jagličić, S. I. Kirin, *Cryst. Growth Des.* **2020**, *20*, 2440.
[30] E. R. Milaeva, V. Y. Tyurin, D. B. Shpakovsky, A. A. Moiseeva, Y. A. Gracheva, T. A. Antonenko, V. V. Maduar, D. I. Osolodkin, V. A. Palyulin, E. F. Shevtsova, *J. Organomet. Chem.* **2017**, *839*, 60.
[31] V. Y. Tyurin, A. A. Moiseeva, D. B. Shpakovsky, E. R. Milaeva, *J. Electroanal. Chem.* **2015**, *756*, 212.
[32] B. A. Wong, S. Friedle, S. J. Lippard, *J. Am. Chem. Soc.* **2009**, *131*, 7142.
[33] K. R. Gee, Z. L. Zhou, W. J. Qian, R. Kennedy, *J. Am. Chem. Soc.* **2002**, *124*, 776.
[34] J. Y. Gerasimov, R. Gabrielsson, R. Forchheimer, E. Stavrinidou, D. T. Simon, M. Berggren, S. Fabiano, *Adv. Sci.* **2019**, *6*, 1801339.
[35] D. Mantione, E. Stavrinidou, E. Pavlopoulou, E. Istif, G. Dufil, L. Vallan, D. Parker, C. Brochon, E. Cloutet, G. Hadziioannou, M. Berggren, *ACS Appl. Electron. Mater.* **2020**, *2*, 4065.
[36] J. Pham, A. Forget, N. Bridonneau, G. Mattana, E. Stavrinidou, S. Zrig, B. Piro, V. Noel, *Electrochem. commun.* **2022**, *137*, 107270.
[37] Y. Mikata, T. Fujimoto, T. Fujiwara, S. I. Kondo, *Inorganica Chim. Acta* **2011**, *370*, 420.
[38] Hammerich, O. & Lund, H. *Organic Electrochemistry*. (CRC Press, 2000). doi:10.1201/9781420029659
[39] F. Panzer, H. Bässler, A. Köhler, *J. Phys. Chem. Lett.* **2017**, *8*, 114.
[40] M. Skompska, A. Szkurlat, *Electrochim. Acta* **2001**, *46*, 4007.
[41] T. F. Otero, H.-J. Grande, J. Rodríguez, *J. Phys. Chem. B* **1997**, *101*, 3688.
[42] R. Giridharagopal, L. Q. Flagg, J. S. Harrison, M. E. Ziffer, J. Onorato, C. K. Luscombe, D. S. Ginger, *Nat. Mater.* **2017**, *16*, 1.
[43] L. Q. Flagg, L. E. Asselta, N. D'Antona, T. Nicolini, N. Stingelin, J. W. Onorato, C. K. Luscombe, R. Li, L. J. Richter, *ACS Appl. Mater. Interfaces* **2022**, *14*, 29052.
[44] A. Savva, C. Cendra, A. Giugni, B. Torre, J. Surgailis, D. Ohayon, A. Giovannitti, I. McCulloch, E. Di Fabrizio, A. Salleo, J. Rivnay, S. Inal, *Chem. Mater.* **2019**, *31*, 927.
[45] J. O. Guardado, A. Salleo, *Adv. Funct. Mater.* **2017**, *27*, 1701791.
[46] G. Salinas, B. A. Frontana-Uribe, *ChemElectroChem* **2019**, *6*, 4105.
[47] T. Nicolini, A. V. Marquez, B. Goudeau, A. Kuhn, G. Salinas, *J. Phys. Chem. Lett.* **2021**, *12*, 46.
[48] K. Murugappan, M. R. Castell, *Electrochem. commun.* **2018**, *87*, 40.
[49] J. Heinze, A. Rasche, M. Pagels, B. Geschke, **2007**, DOI 10.1021/jp066413p.
[50] S. Inal, G. G. Malliaras, J. Rivnay, *Nat. Commun.* **2017**, *8*, 1767.
[51] M. J. Donahue, A. Williamson, X. Strakosas, J. T. Friedlein, R. R. McLeod, H. Gleskova, G. G. Malliaras, *Adv. Mater.* **2018**, *30*, 1705031.
[52] J. Zhang, X. Peng, Y. Wu, H. Ren, J. Sun, S. Tong, T. Liu, Y. Zhao, S. Wang, C. Tang, L. Chen, Z. Chen, *Angew. Chemie Int. Ed.* **2021**, *60*, 25846.
[53] A. Nawaz, Q. Liu, W. L. Leong, K. E. Fairfull-Smith, P. Sonar, *Adv. Mater.* **2021**, *33*, 2101874.
[54] M. Abarkan, A. Pirog, D. Mafilaza, G. Pathak, G. N'Kaoua, E. Puginier, R. O'Connor, M. Raoux, M. J. Donahue, S. Renaud, J. Lang, *Adv. Sci.* **2022**, *9*, 1.